

Robustness and Variability of Neuronal Coding by Amplitude-Sensitive Afferents in the Weakly Electric Fish *Eigenmannia*

GABRIEL KREIMAN,¹ RÜDIGER KRAHE,² WALTER METZNER,² CHRISTOF KOCH,¹ AND FABRIZIO GABBIANI¹

¹Computation and Neural Systems Program, Division of Biology, 139-74 California Institute of Technology, Pasadena 91125; and ²Department of Biology, University of California at Riverside, Riverside, California 92521-0427

Received 10 November 1999; accepted in final form 21 March 2000

Kreiman, Gabriel, Rüdiger Krahe, Walter Metzner, Christof Koch, and Fabrizio Gabbiani. Robustness and variability of neuronal coding by amplitude-sensitive afferents in the weakly electric fish *Eigenmannia*. *J Neurophysiol* 84: 189–204, 2000. We investigated the variability of P-receptor afferent spike trains in the weakly electric fish, *Eigenmannia*, to repeated presentations of random electric field AMs (RAMs) and quantified its impact on the encoding of time-varying stimuli. A new measure of spike timing jitter was developed using the notion of spike train distances recently introduced by Victor and Purpura. This measure of variability is widely applicable to neuronal responses, irrespective of the type of stimuli used (deterministic vs. random) or the reliability of the recorded spike trains. In our data, the mean spike count and its variance measured in short time windows were poorly correlated with the reliability of P-receptor afferent spike trains, implying that such measures provide unreliable indices of trial-to-trial variability. P-receptor afferent spike trains were considerably less variable than those of Poisson model neurons. The average timing jitter of spikes lay within 1–2 cycles of the electric organ discharge (EOD). At low, but not at high firing rates, the timing jitter was dependent on the cutoff frequency of the stimulus and, to a lesser extent, on its contrast. When spikes were artificially manipulated to increase jitter, information conveyed by P-receptor afferents was degraded only for average jitters considerably larger than those observed experimentally. This suggests that the intrinsic variability of single spike trains lies outside of the range where it might degrade the information conveyed, yet still allows for improvement in coding by averaging across multiple afferent fibers. Our results were summarized in a phenomenological model of P-receptor afferents, incorporating both their linear transfer properties and the variability of their spike trains. This model complements an earlier one proposed by Nelson et al. for P-receptor afferents of *Apteronotus*. Because of their relatively high precision with respect to the EOD cycle frequency, P-receptor afferent spike trains possess the temporal resolution necessary to support coincidence detection operations at the next stage in the amplitude-coding pathway.

INTRODUCTION

Variability has long attracted neurophysiologists as a tool to investigate the biophysical mechanisms of sensory processing, the integrative properties of nerve cells, and the encoding schemes used in various parts of the nervous system (Baylor et al. 1979; Hecht et al. 1942; Shadlen et al. 1996; Softky and Koch 1993). Until recently, most work has focused on characterizing the response variability of nerve cells to static stim-

uli, in part because simple measures such as the variance of the number of spikes recorded in long time windows provide universal and effective ways to quantify variability under such conditions (Parker and Newsome 1998).

Most biologically relevant stimuli, however, are not static. Therefore, more recently, investigators have started to characterize the trial-to-trial variability of responses to time-varying, dynamic stimuli in vivo and in vitro (Bair and Koch 1996; Berry et al. 1997; de Ruyter van Steveninck et al. 1997; Mainen and Sejnowski 1995; Mechler et al. 1998; Reich et al. 1997; Stevens and Zador 1998; Warzecha et al. 1998). When temporal variations are sufficiently strong to induce locking of spikes to stimulus transients, measures such as the standard deviation in the spike occurrence times following those transients or the probability of spike occurrence within a given time window from trial to trial may be used to provide a characterization of variability (Bair and Koch 1996; Mainen and Sejnowski 1995). However, these measures are not likely to carry over to more general stimulation conditions, when locking to stimulus transients is absent or less pronounced. An alternative approach consists of extrapolating from the study of static stimuli and to use the variance in the number of spikes observed in short time windows as a measure of variability (referred to as the *spike count variance*) (Berry et al. 1997; de Ruyter van Steveninck et al. 1997; Warzecha and Egelhaaf 1999). Two goals of the present work are to clarify the limits of the spike count variance as a measure of short term variability, and to introduce a new measure of spike time jitter based on recent work by Victor and Purpura (1996, 1997) that should be applicable to a wide range of stimuli, independent of the integrative properties of the investigated neurons.

Eigenmannia is a weakly electric gymnotiform fish of wave type that discharges its electric organ at regular intervals 200–600 times per second. Two types of tuberous sensory afferent nerve fibers convey information about the resulting electrical environment to the brain (Scheich et al. 1973). T-type afferent fibers provide the first stage of a pathway specialized to process phase information, called the timing pathway (Heiligenberg 1991). They fire one spike per electric organ discharge (EOD) cycle, each tightly phase locked to the zero crossings of the EOD and thus signal phase modulations of the electric field.

Address reprint requests to F. Gabbiani (E-mail: gabbiani@klab.caltech.edu).

The costs of publication of this article were defrayed in part by the payment of page charges. The article must therefore be hereby marked "advertisement" in accordance with 18 U.S.C. Section 1734 solely to indicate this fact.

P-type afferents, on the other hand, fire at most one spike per EOD cycle with loose phase locking to the EOD and a probability that increases in direct proportion to the mean amplitude of the field. They thus convey information about amplitude changes of the electric field to higher order neurons in the brain.

While it is well-known that the timing jitter of P-receptor afferent spikes is greater than that of T-type afferents (Scheich et al. 1973), variability in the amplitude pathway has received little quantitative attention. In contrast, variability in the timing pathway has been characterized in considerable detail, revealing the high precision of neurons in encoding phase shifts of the EOD. T-type fibers are able to fire spikes with a precision of approximately 30 μ s (Carr et al. 1986). This precision increases at higher stages of electrosensory processing because of the pooling and averaging of T-type activity across the body surface (Rose and Heiligenberg 1985). Here we focus on the variability of P-type afferents and show that their firing is approximately 100 times less precise. Nevertheless, our results demonstrate that the jitter in P-receptor afferent spike trains lies within the appropriate range to efficiently convey amplitude information to the electrosensory lateral line lobe, the hindbrain nucleus that forms the first central stage of the amplitude coding pathway.

Part of our results has been presented in abstract form (Kreiman et al. 1998).

METHODS

Preparation and electrophysiology

Eigenmannia specimens of 12–20 cm body length were prepared for electrophysiological recordings as described by Wessel et al. (1996) and Metzner et al. (1998). Briefly, the EOD frequency was measured, and subsequently the animal was immobilized and its EOD amplitude attenuated by an intramuscular injection of Flaxedil (galamine triethiodide, Sigma, St. Louis, MO; <5 μ g/g body wt). Under local anesthesia (2% lidocaine, Western Medical Supply, Arcadia, CA), the posterior branch of the anterior lateral line nerve was exposed just rostral to the operculum. Signals from P-receptor afferents were recorded extracellularly from this nerve with glass micropipettes filled with 3 M KCl (resistance: 40–60 M Ω), amplified with an extra/intracellular electrometer (World Precision Instruments 767, Sarasota, FL), and stored on video tape using a PCM recording adapter (Vetter 3000A, Rebersburg, PA; sampling rate: 40 kHz). They were subsequently digitized using a commercial data analysis system (Datawave, Denver, CO; sampling rate: 10 kHz/channel). A few recordings were acquired and digitized using LabView (National Instruments, Austin, TX). Data corresponding to one point in Fig. 13 (for the cutoff frequency $f_c = 88$ Hz, see *Stimulation* below for a complete description) were obtained in a previous study (Wessel et al. 1996).

Stimulation

P-receptor afferents were stimulated as described previously (Metzner et al. 1998; Wessel et al. 1996). A sinusoidal carrier signal (Exact 519, Hillsboro, OR) with a frequency matched to the EOD frequency (f_{EOD}) of the fish was modulated in amplitude. The main difference with earlier work was that electric field AMs were synthesized and stored digitally for playback using commercial software (Signal Engineering Design, Belmont, MA; sampling rate: 2 kHz), allowing for repeated presentations of identical stimuli. The AM and the carrier signal were gated by the same trigger signal and were therefore phase locked to each other. The stimuli were delivered via

two carbon rod electrodes, one positioned either in front of the animal or in its mouth, the other behind its tail. No differences in the neuronal responses were observed between these two configurations. The mean stimulus amplitude, measured at the side fin perpendicular to the body axis, ranged from 1 to 5 mV/cm. To avoid under-driving the afferents, it was adjusted individually for each P-receptor afferent to stimulate it at 10–15 dB above threshold.

One set of stimuli consisted of random AMs (RAMs) with a flat power spectrum (white noise) up to a fixed cutoff frequency ($f_c = 5, 10, 20, 40, \text{ and } 60$ Hz). These AMs were obtained using a modulation signal $s(t)$ that caused a doubling of the carrier signal amplitude for $s(t) = 1$ V and a reduction to zero for $s(t) = -1$ V (see Eq. 1 of Wessel et al. 1996). The standard deviation, σ , of the stimulus $s(t)$ (which can be thought of as the stimulus contrast) was varied between 10 and 30% of the mean electric field amplitude ($\sigma = 100, 150, 200, 250, 275, \text{ and } 300$ mV; $\sigma = 1$ V corresponded to a 100% variation of the stimulus amplitude). Consequently, amplitudes varied over a range of -20 to -10 dB of the mean stimulus amplitude. A single 15-s-long stimulus was synthesized for each parameter pair (f_c, σ) and was presented 10 times, drawn in pseudo-random order from a subset of all possible (f_c, σ) combinations. We usually started by presenting all f_c values at a fixed contrast ($\sigma = 250$ mV) or all contrasts at two cutoff frequencies ($f_c = 5, 60$ Hz). Further (f_c, σ) combinations were tested as time permitted.

The second set of stimuli consisted of sinusoidal AMs (SAMs) at a fixed contrast ($\sigma = 250$ mV) and at various temporal frequencies f_s . The values used were $f_s = 0.1, 0.5, 1, 5, 7, 10, 20, 50, 100, \text{ and } 125$ Hz. Each stimulus was 15 s long and was presented six times in pseudo-random order. These stimuli were presented interleaved with the RAMs protocol described above.

Characterization of spike train variability

Two methods were used to quantify inter-trial spike train variability in response to repeated presentations of the same RAM stimulus. We first computed the spike count variance as a function of the mean spike count in fixed time windows of length T (see RESULTS and Fig. 5). The same RAM stimulus was presented $R = 10$ times and the number of spikes, n_i , occurring in a fixed time window, T , was determined for each trial $i = 1, \dots, R$. The average number of spikes occurring in that window, $\langle n \rangle$ (mean spike count), and its variance, $\sigma_{\langle n \rangle}^2$ (spike count variance), were estimated from

$$\langle n \rangle = \frac{1}{R} \sum_{i=1}^R n_i \quad \sigma_{\langle n \rangle}^2 = \frac{1}{R-1} \sum_{i=1}^R (n_i - \langle n \rangle)^2$$

Three window sizes were used ($T = 10, 50, \text{ and } 100$ ms), and each time window was successively shifted by 5 ms to cover the entire stimulus presentation interval. For highly variable spike trains, such as those corresponding to independent Poisson-distributed spike occurrence times, the spike count variance equals the mean independent of the window T . Conversely, if the $R = 10$ spike trains are exactly identical, $\sigma_{\langle n \rangle}^2 = 0$ in each window T . If, however, the spike trains are not exactly identical, the minimum nonzero variance may be computed by considering the discrete nature of spiking. With f lying in the interval $[0; 1]$, we assume that a fraction $(1 - f)$ of spike counts in a fixed interval of length T equals the integer n_T (where n_T is usually small) and the remaining fraction, f , contains one additional spike, so that the spike counts equal $n_T + 1$. It then follows that the mean spike count, $\langle n \rangle$ (a positive real number), is given by

$$\begin{aligned} \langle n \rangle &= (1 - f)n_T + f(n_T + 1) \\ &= n_T + f \end{aligned}$$

and the minimal variance is

$$\begin{aligned}\sigma_{(n)}^2 &= (1-f)(n_T - \langle n \rangle)^2 + f(n_T + 1 - \langle n \rangle)^2 \\ &= f(1-f)\end{aligned}$$

This last equation states that $\sigma_{(n)}^2$ is a quadratic function of the fraction, f , of spike counts equaling $n_T + 1$ in the interval T . As a function of f , the minimal variance spans a parabola between successive integer values of the mean spike count, taking its maximal value ($=1/4$) at $f = 1/2$ and its minimal value ($=0$) for integer spike counts ($f = 0$; see RESULTS and Fig. 5). Similarly, if all spike counts in T for all R repetitions are equal to n_T or $n_T + 1$ except for one spike count equal to $n_T - 1$ (or $n_T + 2$), then the variance still follows a parabola, but translated by a factor $2/R$ along the vertical axis: $f(1-f) + 2/R$. Successive parabolas translated vertically are generated by an analogous procedure (see RESULTS and Fig. 5).

A second measure of inter-trial variability that proved more sensitive to changes in stimulus parameters (see RESULTS) was obtained by computing an average distance between spike trains obtained in response to the same RAM. The distance measure employed was introduced by Victor and Purpura (1996) based on an earlier one used to quantify the similarity of DNA sequences (Li and Graur 1991, chap. 3; Sellers 1974). Operationally, the distance between two spike trains is defined by the following procedure: the first spike train is transformed into the second one by a series of elementary steps. Each step is assigned a "cost" and the distance is obtained by adding up the cost of all elementary steps and finding the transformation sequence yielding the minimal cost. This procedure is illustrated in Fig. 1: the two spike trains to be compared are labeled 1 and 8, while spike trains 2–7 represent the sequence of elementary steps in the transformation yielding the minimal cost. Only three elementary steps are allowed: adding a spike (as in step 6 to 7), deleting a spike (as in step 1 to 2) or moving a spike to a new position (as in step 2 to 3). The first two elementary steps are assigned an arbitrary cost of 1, whereas moving a spike by Δt ms is assigned a cost of $q \cdot |\Delta t|$ for q positive. Victor and Purpura (1996, 1997) describe an algorithm for determining the minimum cost transformation sequence and derive the mathematical properties of the ensuing distance measure, $d_{ij}(q)$, between two spike trains x_i and x_j . The parameter q (measured in units of 1/time) characterizes the time interval for which the occurrence of a spike in x_i is considered to be significantly different from the occurrence of a spike in x_j : if the interval separating the spikes is larger than $2/q$ it is

less "expensive" to transform x_i into x_j by first deleting the spike in x_i and then adding it in x_j (at a cost of 2) than by translating it to its new position (at a cost of $q \cdot |\Delta t|$; Fig. 1B). It is therefore straightforward to compute $d_{ij}(q)$ when q is large: let n_i and n_j be the number of spikes in x_i and x_j , respectively, and the integer c_{ij} denote the number of coincident spikes in x_i and x_j (coincident within some discretization interval). For large q 's it is always less expensive to delete and add spikes than to move them so that the distance between x_i and x_j is obtained by first deleting $(n_i - c_{ij})$ spikes in x_i and then adding $(n_j - c_{ij})$ spikes in x_j . Thus

$$d_{ij}(q \rightarrow \infty) = n_i + n_j - 2c_{ij} \quad (1)$$

On the other hand, if the cost of moving a spike vanishes, $q = 0$, each spike in x_i may be moved at zero cost to match the position of an arbitrary spike in x_j , and a cost of 1 is only endured for each additional spike to be added or deleted in x_j . Therefore

$$d_{ij}(0) = |n_i - n_j| \quad (2)$$

measures the difference in the number of spikes between the two spike trains. As $q \geq 0$ increases, $d_{ij}(q)$ increases monotonically and reaches its maximum value (given by Eq. 1) when $2/q$ is smaller than the minimal time interval between two noncoincident spikes in x_i and x_j . Note that if the two spike trains are perfectly coincident $d_{ij}(q) = 0$, independent of q . The distance $d_{ij}(q)$ was normalized by the total number of spikes in the two spike trains

$$d_{ij}^n(q) = d_{ij}(q)/(n_i + n_j) \quad \text{with } 0 \leq d_{ij}^n(q) \leq 1 \quad (3)$$

so that $d_{ij}^n(0)$ measures the difference in spike count normalized by the total spike count and $d_{ij}^n(q \rightarrow \infty)$ is the fraction of noncoincident spikes relative to the total number of spikes.

The *effective temporal jitter*, t_{jitter} , of the spike occurrence times was defined as $t_{\text{jitter}} = 1/q_{1/2}$ where $q_{1/2}$ is the value of q such that $d_{ij}^n(q_{1/2}) = 1/2$. This definition is motivated by the following arguments showing that t_{jitter} equals the average time interval, \bar{t}_{inter} , by which spikes are moved to transform one spike train into the other one if no spikes have to be added or deleted (see Eq. 6). Thus the effective temporal jitter t_{jitter} is a generalization of \bar{t}_{inter} to situations where spikes might also need to be added or deleted, as we now explain. For a fixed value of q , let n_α , n_β , and n_γ denote the number of spikes moved, deleted, and added when computing the distance between x_i and x_j . If we pool together all noncoincident spikes in x_i and x_j , $n_i +$

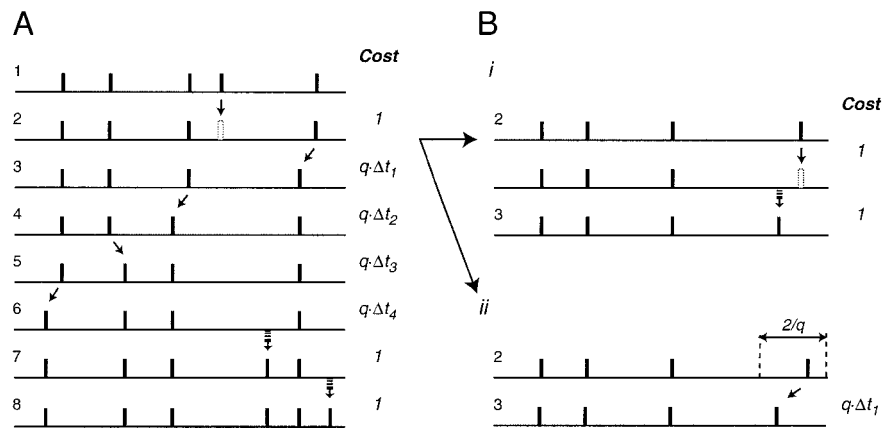


FIG. 1. Computation of spike train distances. The distance between 2 spike trains was obtained as the minimum cost to convert one spike train into the 2nd one using 3 elementary steps. A: the minimum cost path transforming spike train 1 into spike train 8 is illustrated (for a fixed value of q). Each intermediate spike train 2–7 corresponds to one elementary step: moving (from 2 to 3), adding (from 6 to 7) or deleting (from 1 to 2) a single spike. The cost of each elementary step is indicated on the right. Note that the cost of moving a spike is proportional to the distance that it is moved along the time axis. B: there are 2 alternatives to go from spike train 2 to spike train 3 in A: i) delete the last spike and add a new one or ii) move the last spike to its new desired position. The latter alternative is less expensive for the particular value of q illustrated here since $q \cdot |\Delta t_1| < 2$ (the dashed time interval of length $2/q$ corresponds to the maximum displacement for which it is less expensive to move a spike).

$n_j - 2c_{ij}$, then each one of these spikes is either moved, deleted, or created when transforming x_i into x_j so that the following equation holds

$$2n_\alpha + n_\beta + n_\gamma = n_i + n_j - 2c_{ij} \quad (4)$$

Using Eqs. 3 and 4 to express $d_{ij}^n(q)$ directly in terms of n_α , n_β , and n_γ we obtain

$$d_{ij}^n(q) = \frac{\sum_{i=1}^{n_\alpha} q \cdot |\Delta t_i| + n_\beta + n_\gamma}{2n_\alpha + n_\beta + n_\gamma + 2c_{ij}}$$

where $|\Delta t_i|$ is the time interval by which the i th spike (out of n_α) is moved. Therefore when $q = q_{1/2}$, rearranging this last equation shows that the average time interval by which a spike is moved is given by

$$\frac{1}{n_\alpha} \sum_{i=1}^{n_\alpha} |\Delta t_i| = \frac{1}{q_{1/2}} \left(1 - \frac{n_\beta + n_\gamma - 2c_{ij}}{2n_\alpha} \right) \quad (5)$$

Let us assume from now on that the number of coincident spikes is negligible, $c_{ij} = 0$ (see RESULTS). If all spikes are moved to transform one spike train into the other one ($n_\beta = n_\gamma = 0$), Eq. 5 implies that

$$\frac{1}{n_\alpha} \sum_{i=1}^{n_\alpha} |\Delta t_i| = \frac{1}{q_{1/2}} \quad (\text{if } n_\beta = n_\gamma = 0) \quad (6)$$

and $1/q_{1/2}$ is the average time interval, \bar{t}_{inter} , by which spikes are moved. If $n_\beta \neq 0$ and/or $n_\gamma \neq 0$, then the distance by which the remaining n_α spikes are moved is on average smaller to compensate for the extra cost imposed by spike additions and deletions (see Eqs. 4 and 5; the expression within the parentheses in Eq. 5 will be <1). Note, however, that the total number of displaced spikes cannot be less than half the average total number of spikes

$$n_\alpha \geq \frac{1}{2} \cdot \frac{n_i + n_j}{2}$$

since the right hand side of Eq. 5 has to be positive. Thus t_{jitter} provides an appropriate measure of spike time jitter, which automatically takes into account possible spike additions or deletions.

From the responses of a P-receptor afferent to 10 repetitions of a RAM stimulus, we computed an estimate of the average normalized distance between two spike trains as a function of q ,

$$D_n(q) = \frac{1}{n_{\text{pairs}}} \sum_{i=1}^{10} \sum_{j=1, j \neq i}^{10} d_{ij}^n(q) \quad \text{with } 0 \leq D_n(q) \leq 1$$

where $n_{\text{pairs}} = 90$ (n_{pairs} is obtained by considering all possible pairs of trains among 10). Normalized distances were typically computed for $q = 0, 0.05, 0.1, 0.25, 0.5$, and 20 ms^{-1} (the last value corresponds to the temporal resolution, $2/q = 0.1 \text{ ms}$, at which spike occurrence times were digitized). According to Eqs. 1 and 2, $D_n(20)$ measures the average fraction of noncoincident spikes, while $D_n(0)$ measures the average difference in spike counts (normalized by the total spike count). The average effective temporal jitter, $\bar{t}_{\text{jitter}} = 1/\bar{q}_{1/2}$, $D_n(\bar{q}_{1/2}) = 1/2$ measures the average jitter of the spike occurrence times under repeated presentation of the same stimulus. The value of $\bar{q}_{1/2}$ was estimated to ± 0.02 accuracy [i.e., $\bar{q}_{1/2}$ satisfied the requirement: $0.48 < D_n(\bar{q}_{1/2}) < 0.52$] by the bisection method (Press et al. 1992, chapt. 9). The percentage of spikes moved, $n_\alpha/(2n_\alpha + n_\beta + n_\gamma)$, and the percentage of spikes added or deleted, $(n_\beta + n_\gamma)/(2n_\alpha + n_\beta + n_\gamma)$, were computed over 3 s of data and six stimulus repetitions (instead of the 15 s and 10 repetitions used to compute the distances) because this task was computationally very intensive. We verified in a few cases that the results were not altered significantly by this procedure. For this latter task, a total of 15 units and 140 stimulus conditions were analyzed. We checked that the distances $D_n(\bar{q}_{1/2})$

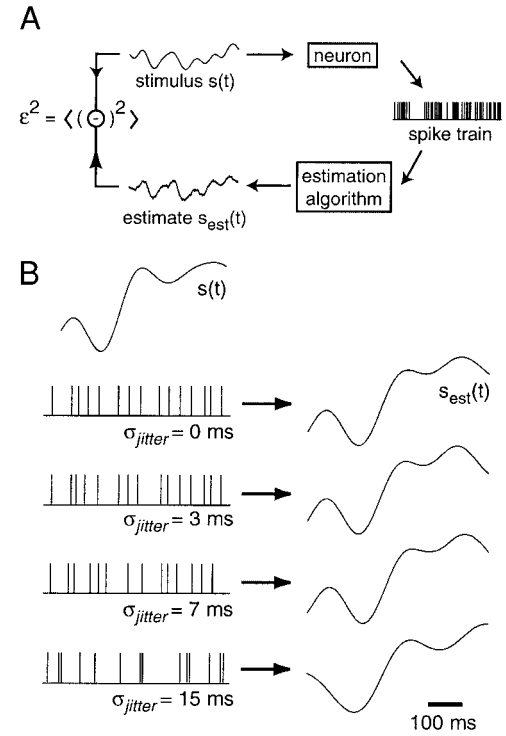


FIG. 2. Quantification of stimulus encoding and of its robustness to spike time jittering. A: an estimate, $s_{\text{est}}(t)$, of the stimulus $s(t)$ was obtained from the spike train by convolving it with a Wiener-Kolmogorov (WK) filter (see main text for details). The accuracy of stimulus encoding by the spike train was assessed by computing the mean square error (ϵ^2) between the stimulus and the estimate. The brackets, $\langle \cdot \rangle$, denote averaging over time. B: temporal jitter was introduced by adding to each spike time a random variable taken from a zero-mean gaussian distribution with standard deviation σ_{jitter} . The modified spike trains are shown for increasing values of σ_{jitter} (from top to bottom) on the left. From each distorted spike train, a new WK-filter and a new estimate, $s_{\text{est}}(t)$, of the stimulus were computed (right). Robustness was quantified by computing the rate at which the fraction of the stimulus encoded decreased with σ_{jitter} (see inset to Fig. 13). A similar procedure was used when spikes were randomly added or deleted from the spike trains.

computed over these reduced data sets lay between 0.45 and 0.55. This was the case for 125 stimulus conditions; the other 15 conditions were not considered further.

Stimulus estimation

The accuracy of single P-receptor afferent spike trains in encoding RAMs was assessed by linearly estimating the stimulus from the recorded spike trains. This technique essentially replaces each spike in a spike train by a continuous waveform, $h(t)$, thus yielding an estimate, $s_{\text{est}}(t)$, of the stimulus, $s(t)$ (Fig. 2A). The waveform $h(t)$ is chosen to optimize the match between $s_{\text{est}}(t)$ and $s(t)$ and, at low firing rates, it closely resembles the mean stimulus waveform preceding a spike (Gabbiani and Koch 1996; Wessel et al. 1996). The theoretical aspects of this signal processing technique and its application to P-receptor afferent spike trains have been discussed in detail elsewhere (Gabbiani and Koch 1998; Wessel et al. 1996; see also Gabbiani and Metzner 1999 for an introduction). For each spike train $x_i(t)$ ($i = 1, \dots, 10$) obtained on presentation of a RAM $s(t)$, we subtracted the mean firing rate and estimated the filter, $h_i(t)$, that minimizes the mean square error between the stimulus and the estimated stimulus obtained by convolving $h_i(t)$ with $x_i(t)$ (see Fig. 2A). This filter is called a Wiener-Kolmogorov (WK) filter in the signal processing literature (e.g., Poor 1994) and plays a role analogous to the impulse response used to estimate the instantaneous firing rate of a neuron (see

Fig. 1 of Gabbiani and Metzner 1999). Each estimate of the WK filter depends on the recorded spike train $x_i(t)$ from which it is computed and is therefore indexed accordingly as $h_i(t)$. The WK filter was computed using MATLAB M-files (The MathWorks, Natick, MA) available at the following web address: <http://www.klab.caltech.edu/~gabbiani/signproc.html>. We then estimated the mean square estimation error, ϵ^2 , by cross-validation (Fukunaga 1990): each filter $h_i(t)$ was convolved with a spike train $x_j(t)$ different from the one used to compute $h_i(t)$ to avoid over fitting. This yielded an estimate $\hat{\epsilon}_{ij}^2$

$$\hat{\epsilon}_{ij}^2 = \langle [s(t) - (h_i * x_j)(t)]^2 \rangle \quad i = 1, \dots, 10, j = 1, \dots, 10, i \neq j$$

where the brackets, $\langle \cdot \rangle$, denote time-averaging and $*$ denotes the time convolution operation (Gabbiani and Koch 1998). An improved estimate was obtained by averaging over all possible pairs

$$\epsilon^2 = \frac{1}{n_{\text{pairs}}} \sum_{i=1}^{10} \sum_{\substack{j=1 \\ j \neq i}}^{10} \hat{\epsilon}_{ij}^2$$

where $n_{\text{pairs}} = 90$. The fraction of the stimulus encoded, or coding fraction, was evaluated as

$$\gamma = 1 - \frac{\epsilon}{\sigma}$$

where σ is the standard deviation of the stimulus. In the worst possible case, when the spike train is completely uncorrelated with the stimulus, the linear estimation algorithm predicts the stimulus mean value and the root mean square error equals the stimulus standard deviation. The root mean square error is therefore always smaller than the stimulus standard deviation ($\epsilon \leq \sigma$) so that the coding fraction, γ , lies between 0 and 1. The coding fraction represents the fraction of the stimulus, expressed in units of σ , that can be reconstructed by linear filtering of the spike train.

Robustness of RAM encoding to spike time jitter, and random spike additions or deletions

To investigate the effect of spike time jitter, spike failures and the occurrence of spikes unrelated to the stimulus on the encoding of RAMs by P-receptor afferents, we created synthetic spike trains from the experimental ones by randomly adding, deleting or jittering spikes (Bialek et al. 1991). The stimulus was then estimated from these

synthetic spike trains, and the coding fraction was monitored as a function of the parameters determining the amount of jitter and the number of spikes added or deleted. Each one of these three types of modifications was introduced separately. In all cases, a minimum separation of 2 ms was imposed between two spikes of the modified spike trains to take into account the refractory period of the afferent fibers.

Let p_{add} indicate the percentage of spikes added to the experimental spike train and p_{del} the percentage of spikes randomly deleted. For spike time jittering, the spikes were moved from their actual occurrence times by a random distance taken from a zero-mean gaussian distribution with various standard deviations σ_{jitter} (Fig. 2B). We used $\sigma_{\text{jitter}} = 0, 1, 3, 5, 7, 10, 15$, and 30 ms; $p_{\text{add}} = 0, 1, 5, 10, 20$, and 30%; $p_{\text{del}} = 0, 1, 5, 10, 20$, and 30%.

Let $\gamma(p_{\text{add}})$, $\gamma(p_{\text{del}})$, and $\gamma(\sigma_{\text{jitter}})$ denote the coding fractions for a given value of p_{add} , p_{del} , and σ_{jitter} , respectively. The robustness of RAM encoding by P-receptor afferent spike trains was evaluated by plotting the normalized coding fraction $\gamma_n(x) = \gamma(x)/\gamma(0)$ where $x = p_{\text{add}}, p_{\text{del}}$, or σ_{jitter} as a function of x (Fig. 13, inset). In most cases, the normalized coding fraction was linearly related to the distortion parameter x (see RESULTS). We therefore performed linear fits of γ_n as a function of $x = p_{\text{add}}, p_{\text{del}}$, or σ_{jitter}

$$\gamma_n(p_{\text{add}}) = 1 + \alpha_{\text{add}} \cdot p_{\text{add}}$$

$$\gamma_n(p_{\text{del}}) = 1 + \alpha_{\text{del}} \cdot p_{\text{del}}$$

$$\gamma_n(\sigma_{\text{jitter}}) = 1 + \alpha_{\text{jitter}} \cdot \sigma_{\text{jitter}}$$

where α_{add} , α_{del} , and α_{jitter} are the slopes of the regression lines. The robustness was defined as the amount of distortion required to cause a 50% drop in coding fraction

$$p_{\text{add}}^{50} = \frac{-1}{2 \cdot \alpha_{\text{add}}} \quad p_{\text{del}}^{50} = \frac{-1}{2 \cdot \alpha_{\text{del}}} \quad \sigma_{\text{jitter}}^{50} = \frac{-1}{2 \cdot \alpha_{\text{jitter}}}$$

The values of p_{add}^{50} , p_{del}^{50} , and $\sigma_{\text{jitter}}^{50}$ were obtained by linear interpolation between adjacent values of the normalized coding fraction plotted as a function of the perturbation or by extrapolation at low stimulus cutoff frequencies (see the point $f_c = 5$ Hz in Fig. 13).

Modeling of P-receptor afferent spike trains

Modeling of P-receptor afferent spike trains was performed in three steps. In the first step, the variability of P-receptor afferent spike trains

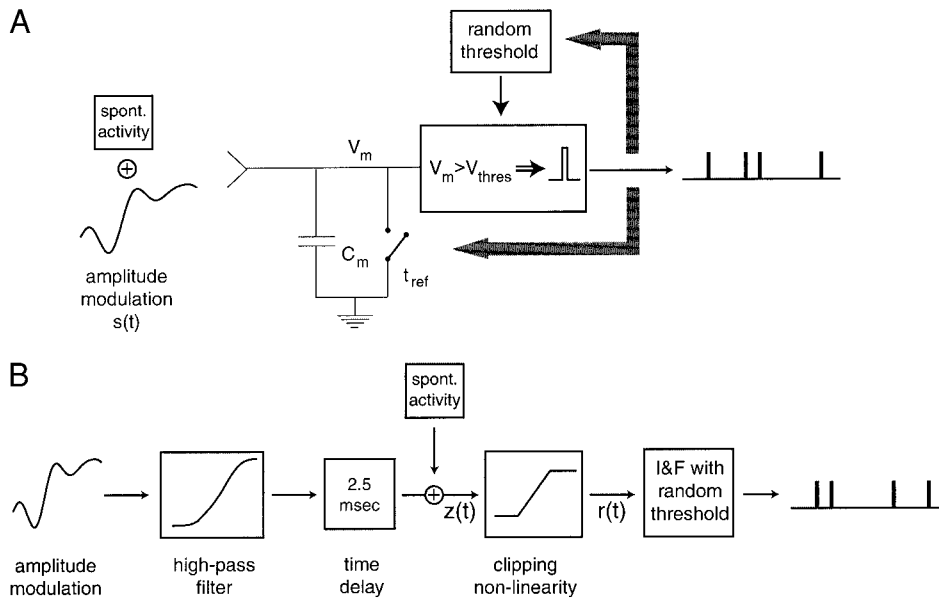


FIG. 3. Comparison of P-receptor afferent spike trains to integrate-and-fire models. A: the variability of experimental spike trains was compared with the variability of perfect integrate-and-fire (I&F) neurons with a random threshold. In this model, the sum of the stimulus and a constant bias term (corresponding to the spontaneous activity) is integrated, and a spike is emitted each time that the threshold (V_{thres}) is reached. After each spike, a refractory period of 2 ms is imposed and a new threshold value is chosen from a gamma probability distribution. B: to model the linear transfer properties of P-receptor afferent spike trains, the AM was first linearly filtered, with a high-pass filter fitted from the responses of P-receptor afferent to sinusoidal AMs (SAMs; see Fig. 14) and then delayed. The output $z(t)$ was clipped and injected into a perfect I&F neuron with random threshold and refractory period equal to 2 ms.

during RAM stimulation was compared with that of standard non-leaky integrate-and-fire models with a random voltage threshold (Fig. 3A) (Gabbiani and Koch 1998; Reich et al. 1997). The properties of the model random threshold determine the variability of the resulting spike trains. The random threshold was taken from a gamma distribution with parameters n and V_{th}

$$p_n(V) = c_n \frac{e^{-nV/V_{th}} V^{n-1}}{V_{th}^{n-1}}$$

where

$$c_n = \frac{n^n}{(n-1)! V_{th}}$$

Larger values of n correspond to more reliable spike trains (see RESULTS and Fig. 7) (see also Gabbiani and Koch 1998, Fig. 9.3), and the mean voltage threshold V_{th} determines the mean firing rate of the model. An absolute refractory period of 2 ms was inserted after each spike occurrence. The order of the gamma distribution was varied between 1 (corresponding to an exponential distribution leading to Poisson distributed spike times), 3, 5, 10, and 100 (effectively implementing the limit $n \rightarrow \infty$, which corresponds to a perfect integrator). The mean voltage threshold value, V_{th} , was fixed so as to match the mean firing rate of the model to the one of each P-receptor afferent. Ten repetitions of the same RAM were used to stimulate P-receptor afferents were fed to each model, and the distances between spike trains were computed as explained above.

In the second step, the linear transfer properties of P-receptor afferents were characterized using a model based on an earlier one proposed by Nelson et al. (1997) for P-receptor afferents of *Apterionotus leptorhynchus* (see Fig. 3B). An alternative biophysical model proposed by Kashimori et al. (1996) was not considered here, as our goal was to obtain the simplest possible description of P-receptor afferent spike trains taking into account their linear transfer function and the variability of their spike trains. The stimulus was passed through a first-order high-pass filter with transfer function $H(s)$

$$H(s) = \frac{G_a s}{s + 1/\tau_a} + G_c \quad (7)$$

simulating the linear transfer properties of P-receptor afferents. In this equation, G_a and G_c are gain and offset terms, respectively, τ_a is the time constant of the filter and $s = i\omega = 2\pi if$ is the complex circular frequency of the input signal. The parameters G_a , G_c , and τ_a were obtained by fitting the gain $G(f) = |H(2\pi if)|$ and the phase $\phi(f) = \tan^{-1}[\text{Im}H(2\pi if)/\text{Re}H(2\pi if)]$ of the model to experimentally measured gains and phases obtained from responses to SAMs. For each SAM stimulus, the mean instantaneous firing rate was computed over the full stimulus cycle and fitted to the function

$$mfr(t) = G_{fs} \sin(2\pi f_s t + \phi_{fs}) + c \quad (8)$$

(see RESULTS and Fig. 14). The fit parameters G_{fs} and ϕ_{fs} are the experimental gain and phase at the frequencies f_s used in the SAMs protocols, respectively (see *Stimulation* above). The constant c represents an offset between stimulus and response.

In the third and last step, the variability characterized in the first step and the linear filtering properties obtained in the second step were combined to obtain a complete model reproducing both the variability of P-receptor afferents and their linear filtering properties. The high-pass filtered signal was delayed by 2.5 ms (corresponding to the synaptic delay between tuberous receptors and afferent fibers), and a mean spontaneous activity was added (Nelson et al. 1997) (see Fig. 3B). The resulting signal, $z(t)$, was then passed through a clipping nonlinearity, effectively half-wave rectifying it, and imposing a maximal firing rate of 1 spike per EOD cycle

$$r(t) = \begin{cases} 0 & \text{if } z(t) < 0 \\ z(t) & \text{if } 0 \leq z(t) \leq f_{EOD} \\ f_{EOD} & \text{if } z(t) \geq f_{EOD} \end{cases}$$

The output, $r(t)$ (see Fig. 3B), was fed as input to a perfect integrator with gamma-distributed threshold, as described above, to determine when a spike was fired. The order n of the gamma distribution for the threshold was selected to match the spike train variability in response to SAMs, as assessed by computing interspike interval distributions and distances between spike trains (see above and Gabbiani and Koch 1998). The responses to RAM stimuli, when available, were then compared with the model predictions (see RESULTS). In some cases the mean firing rate of the model was adjusted to take into account changes in the experimental firing rate during a recording session.

RESULTS

This study is based on recordings and analysis from 69 P-receptor afferent fibers obtained in 34 different animals.

Responses of P-receptor afferents to repeated presentations of identical RAMs

To investigate the variability of P-receptor afferent spike trains and its relation to the encoding of electric field AMs, we recorded their responses to repeated presentations of identical RAMs of a sinusoidal electric field. The mean firing rates of afferent fibers were widely distributed, ranging from 25 spike/s to 374 spike/s (117 ± 69 spike/s, mean \pm SD). The coefficient of variation of the interspike interval (ISI) distribution ($CV = \text{mean}/SD$) ranged from 0.16 to 1.7 (0.59 ± 0.36 , mean \pm SD). These values were similar to those observed in spontaneously active units (range: 0.12–1.12) (Wessel et al. 1996, Fig. 2B2), although several units analyzed here had higher CVs under RAM stimulation than those observed spontaneously.

Figure 4 illustrates the range of responses to repeated RAMs recorded under a variety of stimulus conditions and mean firing rates. In a few cases, the responses of P-receptor afferents were highly reproducible from trial to trial (see in particular Fig. 4C and, to a lesser extent, Fig. 4D) as has sometimes been observed in other preparations (Bair and Koch 1996; Berry and Meister 1998; Mainen and Sejnowski 1995). A clear locking of the responses to the stimulus was usually observed at high contrasts ($\sigma > 200$ mV) and cutoff frequencies ($f_c > 40$ Hz; see Fig. 4, C and D). Furthermore, the mean firing rate of the afferent fibers had to be low (< 125 spike/s; compare Fig. 4, C and G). Decreasing the cutoff frequency or the stimulus contrast tended to decrease the reproducibility of the spike occurrence times (Fig. 4, A and B). At high firing rates (> 125 spike/s), P-receptor afferent responses did not show clear trends of changes in reproducibility with stimulus parameters (Fig. 4, E–H). These preliminary observations suggested that the variability across trials of P-receptor afferent spike trains depended on stimulus parameters as well as on the mean firing rate of the units.

Quantification of response variability

The spike count variance over short time windows has often been considered as an indicator of spike train variability across repeated trials of the same stimulus (Berry et al. 1997; de Ruyter van Steveninck et al. 1997). As a first step in quantifying P-receptor afferent spike train variability, we therefore

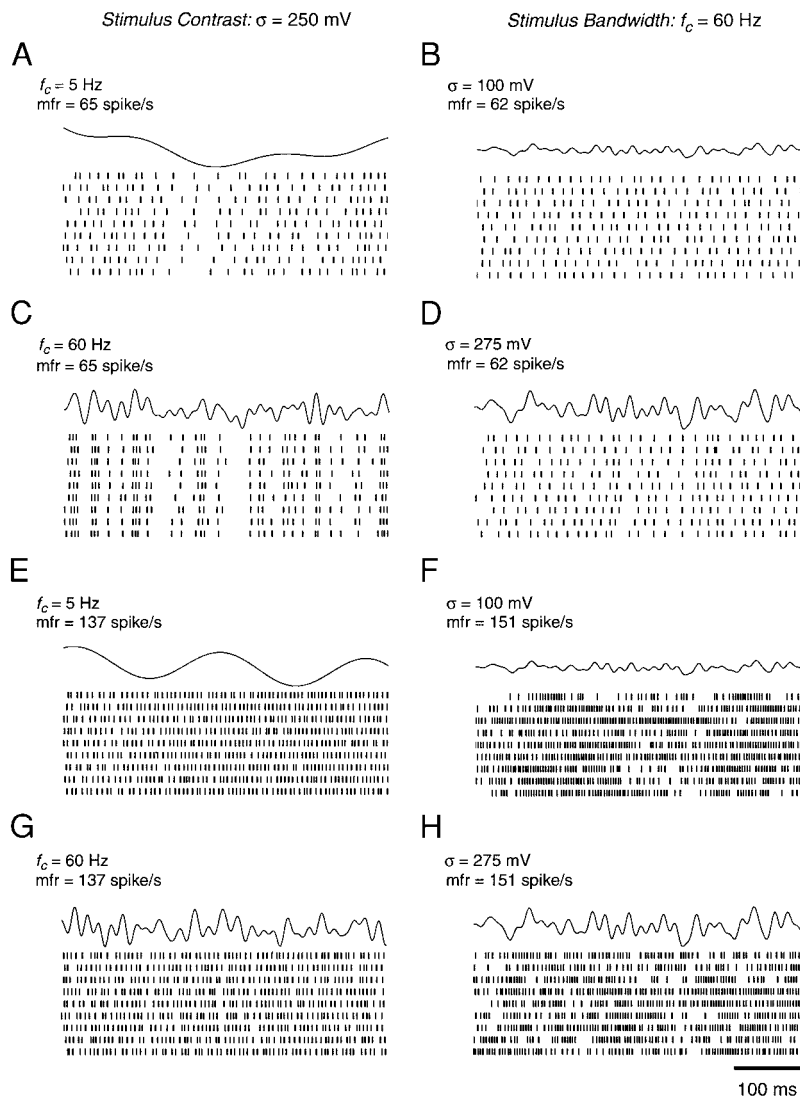


FIG. 4. P-receptor afferent responses to RAMs exhibit a broad range of variability. A portion of the stimulus presented to each P-receptor afferent is shown on *top*. Each raster of spikes (9 per panel, 500 ms long) illustrates the response of the same P-receptor afferent to a single presentation of the stimulus. The *left column* (A, C, E, and G) illustrates responses for fixed stimulus contrast ($\sigma = 250$ mV) of a neuron with low mean firing rate (A and C: mfr = 65 ± 2 spikes/s) and a different neuron with high firing rate (E and G: mfr = 137 ± 1 spikes/s) to stimuli with low and high cutoff frequencies (A and E: $f_c = 5$ Hz; C and G: $f_c = 60$ Hz). The *right column* (B, D, F, and H) illustrates the responses for a fixed cutoff frequency ($f_c = 60$ Hz) of a neuron with low firing rate (B and D: mfr = 62 ± 1 spikes/s) and a different neuron with high firing rate (F and H: mfr = 151 ± 1 spikes/s) to stimuli with low and high contrasts (B and F: $\sigma = 100$ mV; D and H: $\sigma = 275$ mV).

plotted the spike count variance versus mean spike count across trials in windows of various sizes (10, 50, and 100 ms) as illustrated in Fig. 5. At low firing rates (Fig. 5, *top row*) the observed mean spike count in a given window was typically

low (<10 spikes per window), and the variance across trials as a function of the mean had a scalloped appearance, reproducing almost perfectly a series of parabolas stacked onto each other along the vertical axis. Similar observations have been

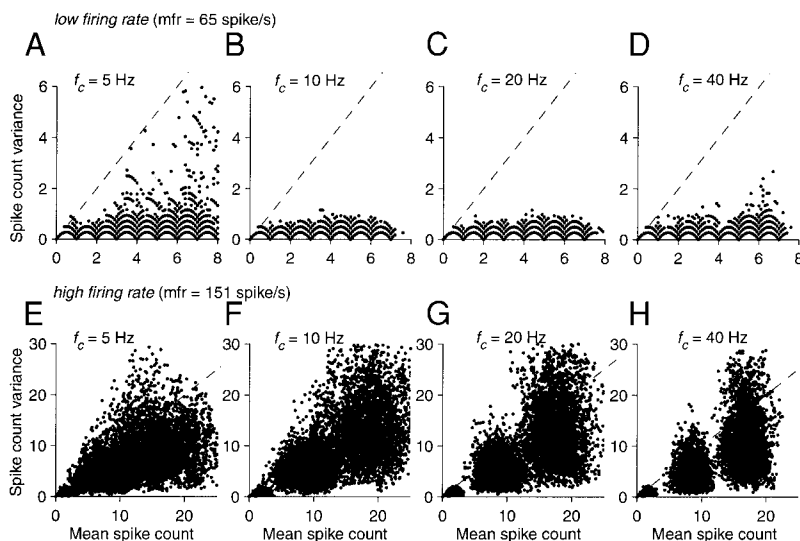


FIG. 5. Scalloping of the variance vs. mean spike count relation is not a predictor of spike timing variability. Plots of spike count variance vs. mean spike count in windows T of 10, 50, and 100 ms. A–D were obtained in a neuron firing at low rate (mfr = 65 ± 2 spikes/s) for fixed contrast ($\sigma = 250$ mV) and various cutoff frequencies f_c (as indicated on the *top* of each panel; A is the same experiment as in Fig. 4A). E–H were obtained in a different neuron with high firing rate (mfr = 151 ± 1 spikes/s) for the same contrast and cutoff frequency values. Note that the variance vs. mean spike count curves follow the theoretical minimum curves in A–D in spite of the fact that reliable spike timing was only observed at high f_c s (see Fig. 4, A–D). At higher firing rates (E–H), scalloping is still observed in some cases but is masked by a general increase in spike count variability. The 3 clusters evident in G and H, and to a lesser extent in F, correspond to the 3 window sizes (if T varies continuously between 10 and 100 ms, no clusters are observed). In all panels, mean equal to variance is indicated by a straight dashed line.

made in other preparations [in ganglion cells of the salamander retina (Berry and Meister 1998); in a wide-field visual tangential neuron of the fly lobula plate (de Ruyter van Steveninck et al. 1997)]. The lowest series of parabolas corresponded to the minimal possible variance that is achieved when the spike count is either equal to n or $n + 1$ (where n is an integer) in a given window (see METHODS). Higher parabolas corresponded successively to all spike counts equal to n or $n + 1$, except for one equal to $n - 1$ (or $n + 2$), etc. . . per window. This result indicated that the number of spikes per window was reliable (either n , $n + 1$, or $n - 1$) and well below that expected for a Poisson process (mean equals variance; dashed line in Fig. 5). However, since the scalloping was observed independently of the stimulus cutoff frequency, it did not correlate with the reliability of spike occurrence times, as observed in spike rasters (see Fig. 4, A–D). At higher firing rates, the mean spike count reached up to 25 spikes or more per window (Fig. 5, bottom row), and the variance increased considerably, ranging from the theoretical minimum up to the mean equals variance line. On average, the variance was still below that of a Poisson process.

Thus according to the experimental results plotted in Fig. 5, scalloping did not appear to be directly related to the precision of spike timing across trials. To confirm this point, we artificially modified the spike trains obtained in response to repeated presentations of identical RAMs to alter the precision in spike timing without changing the statistical properties of the spike trains. We took the 10 rasters of units exhibiting scalloping of the spike count variance versus mean spike count relation and firing with varying degrees of reliability in response to RAMs (such as the rasters for the unit illustrated in Figs. 4, A and C, and 5, A–D) and successively shifted the spikes with a fixed delay t_{shift} . In other words, if $x_1(t), \dots, x_{10}(t)$ represent the original spike trains, new spike trains were defined as $\tilde{x}_1(t) = x_1(t)$, $\tilde{x}_2(t) = x_2(t + t_{\text{shift}})$, \dots , $\tilde{x}_{10}(t) = x_{10}(t + 9 \cdot t_{\text{shift}})$. The parameter t_{shift} took three values: 1, 5, and 10 ms. We then computed the variance versus mean relations exactly as in Fig. 5. In all cases (5 units, 14 conditions) and irrespective of whether the timing of spikes was reliable or not, the scalloping remained present, independently of the value of t_{shift} . In some cases the number of vertical rows of parabolas increased with t_{shift} . These points are illustrated in Fig. 6, A and B. Similar results were obtained in integrate-and-fire neuron models as illustrated in Fig. 6, C and D. Thus in the worst case, $t_{\text{shift}} = 10$ ms, the timing of spikes drifted by 90 ms between the first spike train $\tilde{x}_1(t)$ and the last spike train $\tilde{x}_{10}(t)$ without affecting the scalloping in windows of 10, 50, and 100 ms. Since it was possible to largely eliminate any precision in the spike occurrence times from trial to trial without altering the scalloping of the spike count variance, this analysis confirmed that scalloping in these time windows was not related to the reliability of spike occurrence times.

Because the spike count variance as a function of mean spike count did not offer a reliable indication of spike train variability under our experimental conditions, we turned to a second measure based on the calculation of distances between spike trains obtained under repeated RAM stimulation. This measure, $D_n(q)$, depends on a parameter q (in units of 1/time), which determines the temporal precision at which the distance between two spike trains is computed (higher values of q correspond to higher temporal precisions, see METHODS). For

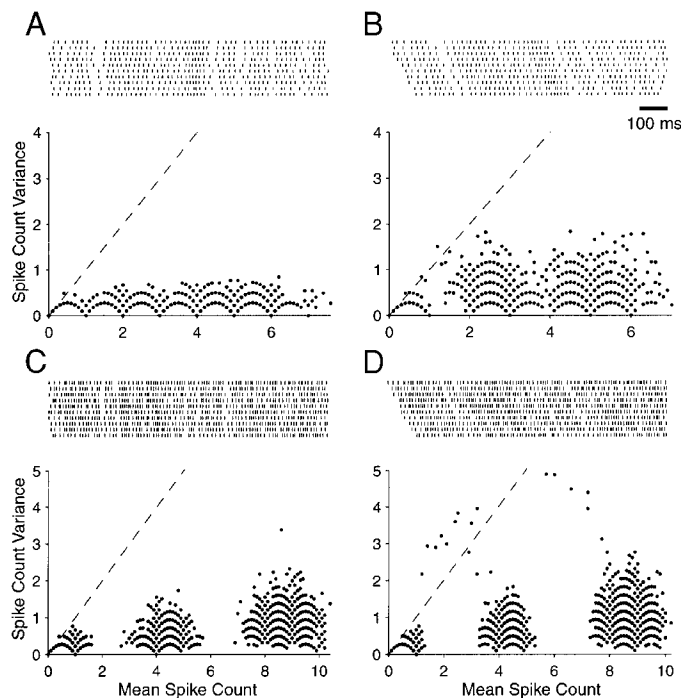


FIG. 6. Scalloping of the variance vs. mean spike count relation measured across trials is preserved even after large shifts in the timing of individual spike trains. A: the top 10 rasters represent the response of a P-receptor afferent ($mfr = 65 \pm 2$ spikes/s; same experiment as in Figs. 4A and 5A) to repeated presentations of a random electric field AM (RAM) stimulus ($\sigma = 250$ mV, $f_c = 10$ Hz). The corresponding spike count variance vs. mean spike count plot is scalloped as illustrated below. B: the spike trains were successively shifted by 10 ms as illustrated on top (see main text), and the variance vs. mean spike count relations was recomputed. Note that the scalloping remained present, although the variance increased as compared with A. C and D: same stimulation and analysis procedure as in A and B for an I&F neuron model with gamma order 10 ($mfr = 81$ spikes/s; see main text and Fig. 7A for a more detailed description of the model).

two identical spike trains $D_n(q) = 0$ independent of q . The maximum, $D_n(q) = 1$, is obtained for large q 's only if no spikes in the two spike trains occurred exactly at the same time. The value at which $D_n(q) = 1/2$, called $\bar{q}_{1/2}$, may be used to summarize spike train variability: if we set $\bar{t}_{\text{jitter}} = 1/\bar{q}_{1/2}$, then \bar{t}_{jitter} measures the average time by which spikes have to be moved to transform one spike train into the second one, or equivalently, the average jitter in spike timing. By definition, this jitter also takes into account differences in spike numbers between the two spike trains (i.e., the need to create or delete spikes to transform one spike train into the other; see METHODS and Fig. 1).

We computed the average distance between all pairs of spike trains obtained in response to the same RAM stimulus for our sample of 69 P-receptor afferents. The spike train distances $D_n(q)$ were compared with those obtained from a family of gamma neuron models indexed by a parameter n controlling spike train variability (see METHODS). A value of $n = 1$ (gamma-1 neuron) corresponds to Poisson-distributed spike occurrence times in response to the stimulus while for large n ($n > 100$) the gamma model is identical to an integrate-and-fire neuron. Figure 7A illustrates in one example how the variability observed in P-receptor afferents compared with the model variability. The top 10 rasters labeled "P-unit" correspond to the response of a P-receptor afferent, while the next 10 rasters

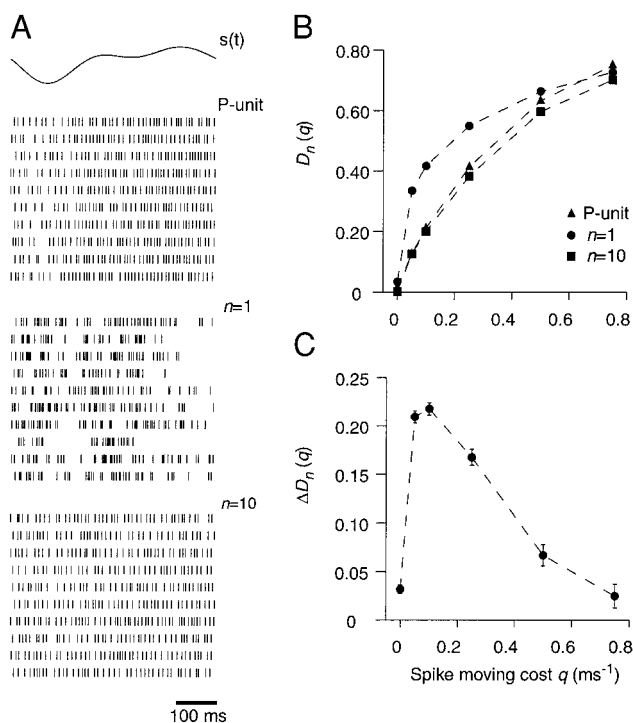


FIG. 7. Spike train distances of P-receptor afferents match those of gamma integrate-and-fire neurons with order n in the 3–10 range. **A**: the spike trains of a P-receptor afferent (top 10 rasters, labeled P-unit; same experiment as in Fig. 5B) recorded in response to a RAM stimulus $[s(t)]$, shown on top, are illustrated together with those elicited by the same stimulus in 2 I&F models with random threshold (labeled $n = 1$ and 10; see Fig. 3A). The $n = 1$ model corresponds to Poisson spike occurrence times and matches poorly the observed variability, while the $n = 10$ model matches it quite well. **B**: plot of the mean distance $D_n(q)$ between 2 spike trains in response to $s(t)$ for the P-receptor afferent and I&F models shown in **A**. The close match between P-unit and $n = 10$ I&F distances confirms quantitatively the visual observation in **A** (standard errors are too small to be visible, $n_{\text{pairs}} = 90$). **C**: plot of the difference in mean distances between $n = 1$ and $n = 10$ models (mean \pm SE, $n_{\text{pairs}} = 90$) as a function of q . $\Delta D_n(q) = D_n(q)_{\text{Poisson}} - D_n(q)_{\text{gamma order 10}}$, where $D_n(q)_{\text{Poisson}}$ corresponds to the filled circles in **B** and $D_n(q)_{\text{gamma order 10}}$ to the squares. Note that the largest difference in distances is observed in the range of q values between 0.05 and 0.25 ms⁻¹. In **B** and **C** the value $q = 20$ ms⁻¹ was not plotted because it would lie off-scale (see main text).

were obtained by simulating a Poisson (gamma-1) model. The P-receptor afferent spike trains are considerably more regular than those of a Poisson neuron and match quite well those of the gamma-10 model illustrated at the bottom of Fig. 7A. Accordingly, the average distance between two spike trains of this P-receptor afferent followed closely those of the gamma-10 neuron (see Fig. 7B, \blacktriangle and \blacksquare) and were always smaller than those of a Poisson model (Fig. 7B, \bullet). The value $D_n(0)$ in Fig. 7B yields the average difference in spike number between two spike trains normalized by the total spike count. The small distance value, $D_n(0) = 0.02$, indicates that the number of spikes was very reproducible from one trial to the next with an average variability of 2%. On the other hand, $D_n(20)$ is the fraction of noncoincident spikes in two spike trains at 0.1-ms resolution. The value $D_n(20) = 0.98$ in this experiment indicates that $<2\%$ of spikes occurred at the same time (± 0.05 ms) and thus the spike trains were clearly not reproducible at a 0.1-ms resolution. The average temporal jitter in spike occurrence times, \bar{t}_{jitter} , was in this case equal to 2.9 ms (with 86% of spikes moved and 14% of spikes added or deleted), corre-

sponding to 1.3 EOD cycles ($f_{\text{EOD}} = 438$ Hz). Furthermore, the largest deviation between $D_n(q)$ in the gamma-10 model (or the P-receptor afferent) and the Poisson model was observed for q values lying in the interval (0.05–0.25 ms⁻¹; Fig. 7C). A value of $q = 0.25$ ms⁻¹ was used to illustrate our results in subsequent figures.

Similar results were obtained in all 69 P-receptor afferents analyzed. The relative difference in spike count, $D_n(0)$, ranged from 0.01 to 0.1 (0.03 ± 0.04 , mean \pm SD), while the fraction of noncoincident spikes, $D_n(20)$, ranged from 0.87 to 1.0 (0.97 ± 0.04). The distribution of average temporal jitters is plotted in Fig. 8A for 69 P-receptor afferents. The range of values was between 0.6 and 23.2 ms (3.5 ± 3.9) with 77 \pm 7% of spikes moved (range: 62–87%) and $23 \pm 7\%$ of spikes added or deleted (range: 13–38%). Figure 8B replots the average temporal jitter in units of the EOD cycle ($1/f_{\text{EOD}}$) as measured for each fish prior to the experiment. The temporal jitter ranged from a fraction of the EOD cycle (0.29) up to several cycles (8.7; 1.4 ± 1.5). The temporal jitter was dependent on the firing rate of the afferent fibers. High firing rate afferents (arbitrarily defined as those with mean firing rate above >125 spike/s) had a mean jitter, \bar{t}_{jitter} , of 1.7 ± 0.3 ms (range: 0.6–2.45 ms) corresponding to 0.8 ± 0.3 EOD cycles (range: 0.3–1.2). The mean jitter of low firing rate afferents (<125 spike/s) was typically higher, 6.3 ± 6.0 ms (range: 1.7–23.2 ms) corresponding to 2.4 ± 2.3 EOD cycles (range: 0.7–8.7).

Dependence of temporal jitter on stimulus cutoff frequency

Next, we investigated the dependence of spike timing jitter on stimulus parameters and P-receptor afferent firing rates.

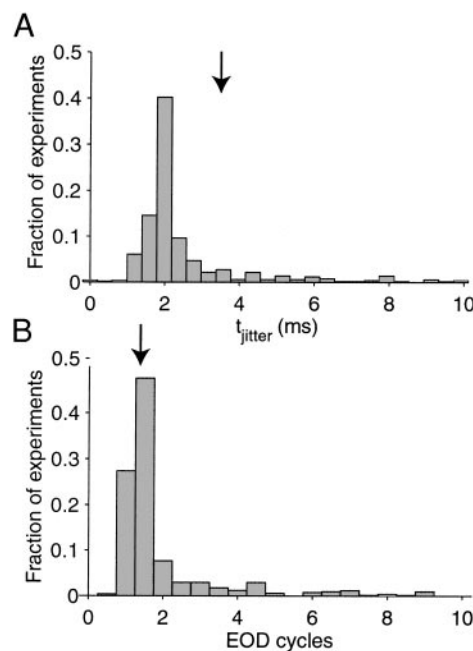


FIG. 8. Distribution of mean spike time jitter on 69 P-receptor afferents (corresponding to 508 different RAM stimulations). **A**: distribution of the average temporal jitter (bin size: 0.4 ms). For display purposes, the probability distribution is shown only up to 10 ms; 8.2% of the cumulative distribution was between 10 ms and the maximal value observed (23.2 ms). **B**: same distribution of \bar{t}_{jitter} in units of electric organ discharge (EOD) cycles (2 bins per EOD cycle). In each panel, the arrows indicate the means of the distributions.

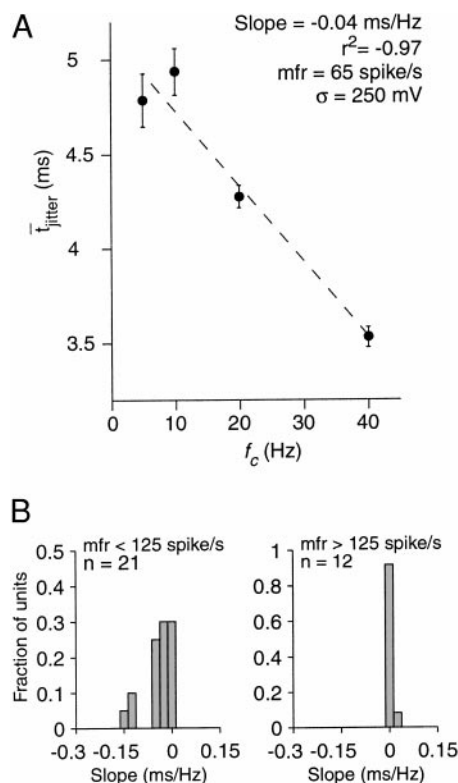


FIG. 9. The timing jitter decreases with stimulus cutoff frequency at low but not at high firing rates. A: plot of the mean jitter in spike occurrence times as a function of stimulus frequency for a neuron firing at low rate (mfr = 65 spikes/s, $\sigma = 250$ mV, $f_{\text{EOD}} = 438$ Hz; percentage of spikes moved: $85 \pm 3\%$). B: the slope of timing jitter vs. cutoff frequency plots (see A) is negative at low firing rates but not at high firing rates. The 2 distributions are significantly different (Wilcoxon rank-sum test, $P < 0.0001$).

Figure 9A illustrates the change in temporal jitter as a function of cutoff frequency for a low firing rate unit (mfr = 65 spike/s). When the stimulus cutoff frequency was increased from 5 to 40 Hz, the timing jitter decreased 1.4-fold from 4.8 to 3.5 ms. This increase in spike timing precision was quantified by the slope of linear regression lines fitted to the data (see Fig. 9A, ---). As illustrated in Fig. 9B, an increase in temporal precision was observed mainly for units firing at low rates. The *left panel* shows the distribution of slopes for units with a mean firing rate below 125 spike/s, and the *right panel* shows the distribution of slopes for units with mean firing rates above 125 spike/s. The slopes calculated for low firing rate units were negative on average (-0.052 ± 0.066 ms/Hz, mean \pm SD) and significantly different from 0 ($P < 0.05$, 2-tailed t -test) while they were not significantly different from zero at high firing rates (0.01 ± 0.02 ms/Hz; $P > 0.4$). Correspondingly, correlation coefficients between f_c and \bar{t}_{jitter} were negative at low rates (-0.59 ± 0.35) but not at high firing rates (0.29 ± 0.62).

Similar results were obtained for the distance measure $D_n(q)$ over a broad range of the spike distance parameter q , as illustrated in Fig. 10. At fixed, intermediate values of q , the average distance decreased as a function of stimulus cutoff frequency for low-firing rate units (Fig. 10, A–C). At low temporal resolution [i.e., when $q = 0$ ms $^{-1}$ and $D_n(q)$ measures differences in spike counts] the slopes and correlation coefficients of $D_n(q)$ versus f_c regression lines were not significantly different from 0 ($P > 0.2$ at $q = 0$ ms $^{-1}$, 2-tailed t -test). That

is, no trend in spike count variability versus stimulus bandwidth could be observed. The same result was true at very high temporal resolution ($P > 0.2$ at $q = 20$ ms $^{-1}$). At intermediate temporal resolutions, units firing at high rates did not show slopes or regression coefficients significantly different from zero (q in the range of 0.05 – 0.75 ms $^{-1}$; $P > 0.05$) while low firing rate units yielded a significant decrease in variability with stimulus bandwidth ($P < 0.01$ over the same range of values). The strongest tendencies were observed for values of q between 0.25 and 0.5 ms $^{-1}$ (Fig. 10, B and C).

Variability and stimulus contrast

The dependence of spike time jitter on stimulus contrast was very similar to the one found for stimulus cutoff frequency.

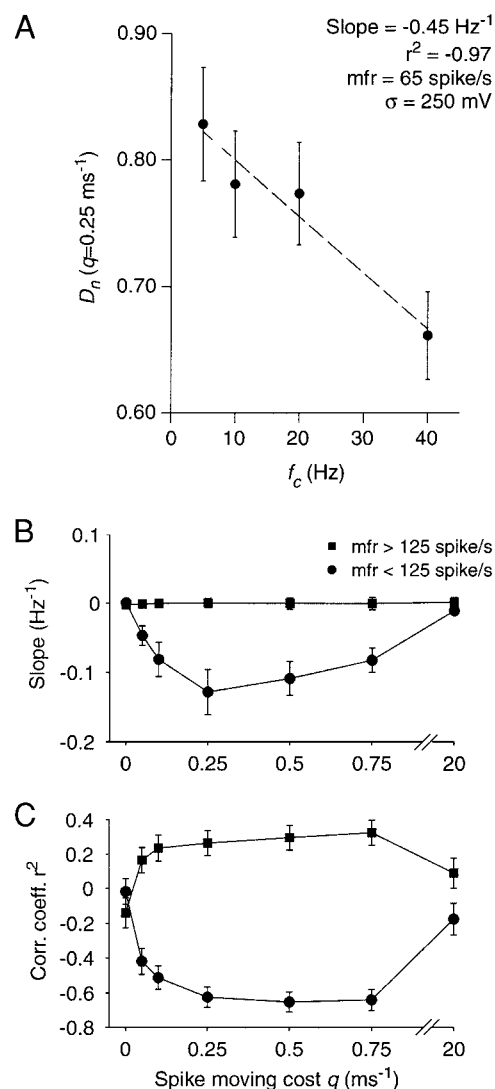


FIG. 10. Increase in timing precision with stimulus cutoff frequency at low but not at high firing rate is observed across a broad range of spike moving costs. A: mean distance between 2 spike trains as a function of cutoff frequency for a value of $q = 0.25$ ms $^{-1}$ ($1/q = 4$ ms) in a low firing rate neuron (mfr = 65 spike/s; $\sigma = 250$ mV). This represents a particularly clear example. B: average slopes (mean \pm SE) of distance [$D_n(q)$] vs. cutoff frequency (f_c) relations (computed as in A) at low (●, average of $n = 21$ neurons) and high (■, average over $n = 12$ neurons) firing rates plotted as a function of q . C: average correlation coefficient (mean \pm SE) of distance vs. cutoff frequency as a function of q (computed as in A).

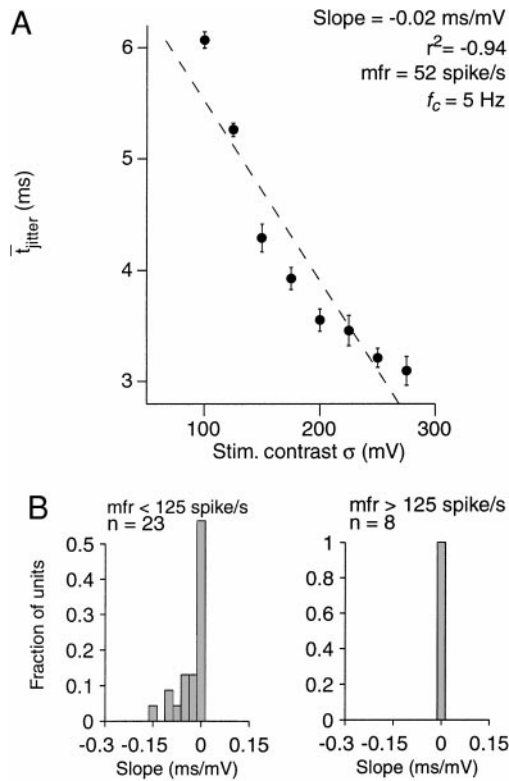


FIG. 11. The timing jitter decreases with increasing stimulus contrast at low but not at high firing rates. **A**: plot of the mean jitter as a function of stimulus contrast for a neuron at low firing rate ($\text{mfr} = 52 \text{ spikes/s}$, $f_c = 5 \text{ Hz}$, $f_{\text{EOD}} = 438 \text{ Hz}$; percentage of spikes moved: $79 \pm 4\%$). **B**: the slope of the timing jitter vs. stimulus contrast relation (see **A**) is negative at low firing rates (*left*, -0.030 ± 0.041) but not at high firing rates (*right*, 0). The 2 distributions are significantly different (Wilcoxon rank-sum test, $P < 0.001$).

Figure 11A illustrates an example of a low firing rate P-receptor afferent for which spike timing jitter decreased two-fold as the stimulus contrast was changed from 10 to 30%. The effect of stimulus contrast on spike timing jitter is summarized in Fig. 11B, which reports the slopes of linear regression lines for \bar{t}_{jitter} versus σ in P-units firing at low and high rates (*left* and *right* panels, respectively). Increasing stimulus contrast was generally less effective than increasing cutoff frequency at reducing spike time jitter as may be seen from the larger fraction of units with slopes close to zero, even at low firing rates.

Figure 12 reports the same results directly in terms of spike train distances at all values of q used. At low firing rates and for intermediate values of the temporal resolution parameter, the average distance between two spike trains decreased as a function of stimulus contrast (Fig. 12A). Accordingly, the slopes of linear regression lines and their correlation coefficients were significantly different from zero for low firing rate units ($P < 0.01$, 2-tailed t -test) but not for high firing rate units ($P > 0.05$) at those values of q (Fig. 12, **B** and **C**). At very low or very high temporal resolution ($q = 0$ or 20 ms^{-1}) changes with stimulus contrast were not statistically significant ($P > 0.05$).

In summary, the study of spike train distances demonstrated that the timing precision of P-receptor afferents increased with stimulus cutoff frequency and, to a lesser extent, with stimulus contrast. Low firing rate units appear to be less variable than high firing rate units.

Robustness of stimulus encoding

To assess the impact of alterations in spike timing on the accuracy of RAMs encoding, we modified experimental spike trains by randomly adding, deleting, or moving spikes. The stimuli were then estimated from the modified spike trains (see Fig. 2B and METHODS), and the change in coding fraction was monitored. The *inset* of Fig. 13 reports in one example the fraction of the stimulus encoded as a function of spike time jitter, normalized by its baseline value, the coding fraction of the original spike train. In most cases the addition and the deletion of spikes or the addition of spike time jitter resulted in a linear decrease of the normalized coding fraction as the

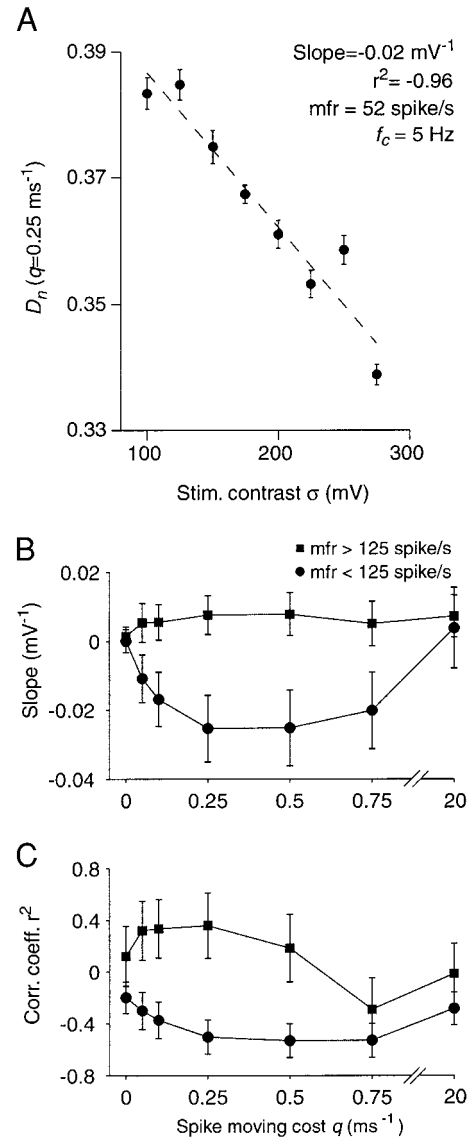


FIG. 12. Increase in timing precision as a function of stimulus contrast is observed at low but not at high firing rates across a broad range of spike moving costs. **A**: mean distance between 2 spike trains as a function of stimulus contrast for a value of $q = 0.25 \text{ ms}^{-1}$ in a low firing rate neuron ($\text{mfr} = 52 \text{ spikes/s}$, $f_c = 5 \text{ Hz}$, $f_{\text{EOD}} = 438 \text{ Hz}$). This represents a particularly clear example. **B**: average slopes (mean \pm SE) of distance [$D_n(q)$] vs. stimulus contrast (σ) relations (computed as in **A**) at low (●, average over $n = 23$ neurons) and high (■, average over $n = 8$ neurons) firing rates as a function of q . **C**: average correlation coefficient (mean \pm SE) of distance vs. cutoff frequency as a function of q (computed as in **A**).

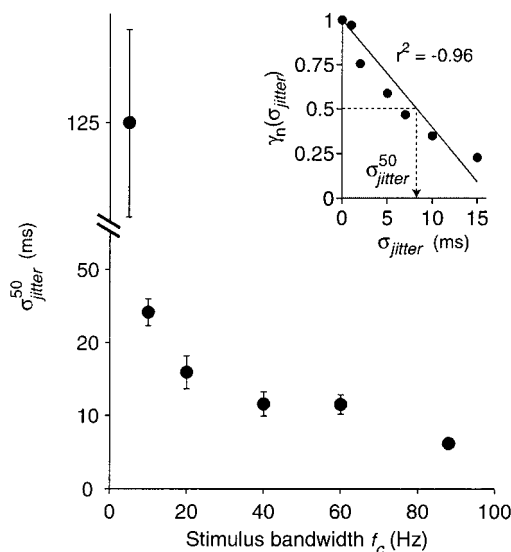


FIG. 13. Robustness of RAM encoding decreases with stimulus bandwidth. Plot of the timing jitter (mean \pm SE) causing a 50% reduction in the coding fraction as a function of stimulus bandwidth. Averages were computed on $n = 58, 38, 21, 22, 38$, and 9 stimulus conditions from low to high f_c , respectively (the large error at $f_c = 5$ Hz is due to extrapolation from shallow slopes, see METHODS and inset for the computation of σ_{jitter}^{50}).

perturbation parameter was increased. Correlation coefficients ranged from 0.80 to 0.97 for 96% of the data. In those cases, the robustness of encoding was characterized by the perturbation value required to cause a 50% drop in coding fraction (see Fig. 13, inset for the definition of σ_{jitter}^{50}). P-receptor afferent spike trains were in general quite robust to such perturbations. As illustrated in Fig. 13, at low cutoff frequencies, spike time jittering as high as 125 ms was required to cause a 50% drop in γ . The robustness to spike time jitter decreased as the stimulus cutoff frequency increased, reaching a value of 6 ms for fast changing stimuli ($f_c = 88$ Hz). The robustness to spike additions or deletions did not show a dependency on stimulus bandwidth for $f_c > 5$ Hz (see Table 1). For those stimuli, a drop of 50% in the coding fraction was obtained after 36% random spike deletions and 41% additions. Robustness was not significantly dependent on stimulus contrast (data not shown).

Modeling of P-receptor afferent variability and linear transfer properties

The results reported above were summarized by building a model of P-receptor afferent spike trains able to account for the encoding of RAMs and the spike train variability observed

experimentally across trials (see Fig. 3 and METHODS). We used an approach similar to the one adopted by Nelson et al. (1997) in modeling P-receptor afferents of *Apteronotus leptorhynchus*. The transfer functions of P-receptor afferents have been described as high pass in the species of weakly electric fish investigated so far (Bastian 1981; Nelson et al. 1997). We confirmed this and characterized quantitatively the transfer function in *Eigenmannia* by recording responses to SAMs. Gains and phases were extracted from linear fits to sinusoids (Fig. 14A and Eq. 8 in METHODS) at various frequencies f_s . The experimental gains and phases were then fitted by maximum likelihood to a first-order high-pass filter (Fig. 14B and Eq. 7). The resulting fits had χ^2 -values divided by the number of degrees of freedoms (χ^2/DOF) (Press et al. 1992, chapt. 15) for the fits between 0.7 and 8.0 (for 15 afferent fibers), except for two outliers ($\chi^2/DOF = 22.8$ and 24.2, respectively). The mean values of the filter parameters were $G_a = 120 \pm 82$ spikes/s (range: 16–300 spikes/s), $G_c = 40 \pm 26$ spikes/s (range: 7–99 spikes/s), and $\tau_a = 4 \pm 5$ ms (range: 0.2–17.5 ms). In contrast to the results of Nelson et al. (1997) in *Apteronotus*, fitting the data with a second-order filter improved only slightly the χ^2/DOF -values of the fits (range: 0.4–6.2). Since the additional parameters were not well constrained, this approach was not pursued further. The static nonlinearity illustrated in Fig. 3B was needed in the model to prevent $z(t)$ from becoming negative, leading to firing rates lower than those observed experimentally. The variability of P-receptor afferent spike trains was estimated from repeated presentations of SAM stimuli and was in the same range as the one observed for RAMs.

The ability of the model to predict responses to RAMs was tested in 10 P-receptor afferents by computing coding fractions and spike train distances as a function of stimulus contrast and cutoff frequency. Figure 15 illustrates two examples for a P-receptor afferent firing at low rate (A–D) and a second P-receptor afferent at high firing rate (E–H). The model successfully reproduced both the dependence of coding fraction and spike train distances observed experimentally on f_c and σ .

DISCUSSION

We characterized the variability of P-receptor afferent responses to RAMs under a variety of stimulus conditions using a new measure of distance between spike trains. Our results provide insight into the relationship between the variance in the number of spikes and the mean spike count as a measure of variability across repeated trials. They also shed light on the impact of variability on the processing of electric field AMs by the electrosensory system in weakly electric fish.

TABLE 1. Robustness to spike time jittering, and random spike additions or deletions

	f_c (Hz)					
	5	10	20	40	60	88
n	58	38	29	21	38	9
p_{add}^{50} , %	72 ± 7	33 ± 3	37 ± 5	37 ± 5	37 ± 4	36 ± 8
p_{del}^{50} , %	91 ± 10	42 ± 3	39 ± 5	42 ± 5	40 ± 5	40 ± 9
σ_{jitter}^{50} , ms	123 ± 9	23 ± 2	16 ± 1	12 ± 1	11 ± 1	6 ± 0.5

Values are means \pm SE; n is number of experiments pooled. Robustness is reported as the amount of noise required for the coding fraction to drop by 50% of its original value (p_{add}^{50} , p_{del}^{50} , and σ_{jitter}^{50}). These values were obtained from a linear interpolation or extrapolation of the normalized coding fraction as a function of the noise level (see METHODS and inset of Fig. 13). Values across different stimulus contrasts were averaged in this table.

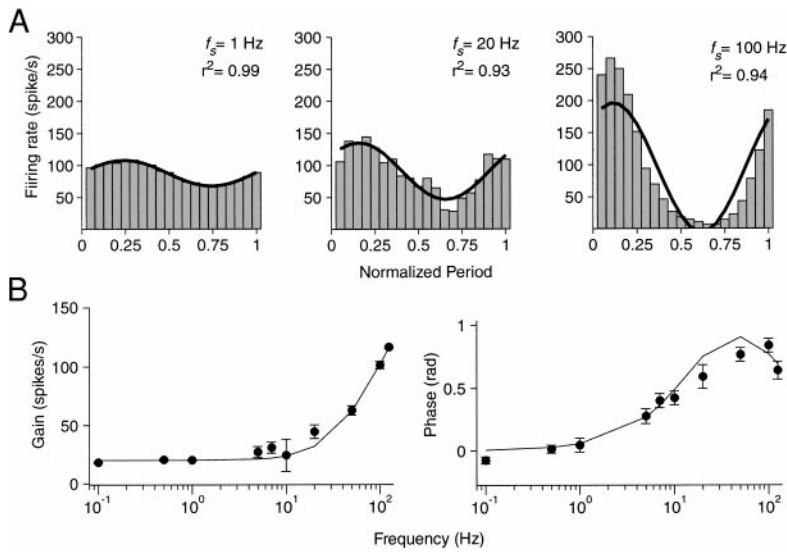


FIG. 14. Fit of linear transfer function properties of a P-receptor afferent by a 1st-order high-pass filter. **A**: plot of the mean instantaneous firing rate as a function of the normalized period fraction p_n ($p_n = t f_s / 2\pi$, bin size: $1/20$ of the period cycle) for 3 different sinusoidal AMs ($f_s = 1, 20$, and 100 Hz, respectively). The solid line represents the fit with Eq. 8 (see METHODS; r^2 is the correlation coefficient between the data and fit). **B**: fits of the mean gain and phase (\pm SD) obtained from **A** (see Eq. 7) with a 1st-order high-pass filter (same neuron as in **A**; fit parameters: $G_a = 147 \pm 9$ spikes/s, $G_c = 20 \pm 2$ spikes/s, $\tau_a = 1.2 \pm 0.8$ ms, $\chi^2/\text{degree of freedom} = 3.2$).

Quantification of spike train variability

Spike train variability has often been quantified by computing the spike count variance as a function of the mean spike count in fixed windows of length T (for a review, see Teich et al. 1996). The benchmark stochastic process to which these values are compared is the Poisson process for which the generation of independent spikes yields a variance equal to the mean. The spike count variance provides an appropriate measure of neural noise in tasks where the mean spike count (averaged over T) is used to assess a neuron's ability to discriminate between two alternatives (for reviews, see Gabbiani and Koch 1998; Parker and Newsome 1998). For long time intervals ($T \geq 1$ s) variances larger than mean spike counts are often observed, indicative of positive long-term correlations in the spike trains (Teich et al. 1996). Such time windows are, however, inadequate to assess the ability of neurons to convey information about time-varying stimuli by rapid changes in instantaneous firing rate.

Recently, the spike count variance has also been used as a measure of variability at short time scales ($T \leq 300$ ms) (Berry et al. 1997; de Ruyter van Steveninck et al. 1997; Warzecha and Egelhaaf 1999). In our data, minimal nonzero values for

the spike count variance were observed in windows smaller than 100 ms, as has been reported in these studies. However, they were not correlated with the reliability of spike occurrence times assessed from raster plots (such as stimulus-dependent phase locking to the sinusoidal carrier signal) or with objective measures of the information encoded in the time-varying firing rate like the coding fraction (Figs. 4–6). Therefore reliable spike timing is not a necessary prerequisite for minimum nonzero variance curves: they may be observed independently of whether spike timing is reproducible at the millisecond level from trial to trial or not. Such curves should therefore be interpreted with caution (see also Barberini et al. 2000; Warzecha and Egelhaaf 1999, footnote 21). One effect leading to variances smaller than the mean over short time windows is the presence of a refractory period that introduces negative correlations between spike occurrence times. The addition of a refractory period to a Poisson stochastic process has recently been shown to be sufficient to account for the variability observed in retinal ganglion cells under dynamic stimulation (Berry and Meister 1998). Similar observations were made in other preparations (for a review, see Johnson 1996). Figure 7B shows that a simple Poisson process with a 2-ms refractory

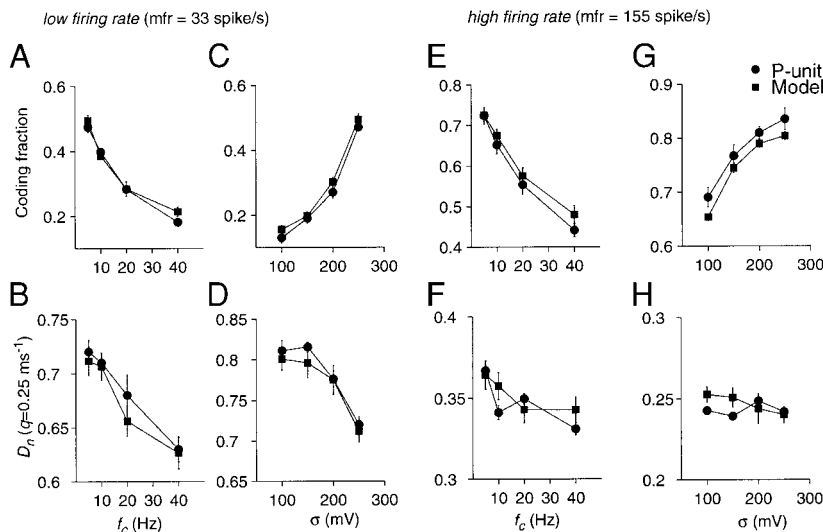


FIG. 15. Comparison of spike train distances and stimulus encoding properties of P-receptor afferents and model. **A** and **E**: coding fraction (mean \pm SE) as a function of stimulus cutoff frequency for 2 different neurons with low and high firing rates, respectively (\bullet) and models (\blacksquare ; $\sigma = 250$ mV). **C** and **G**: coding fraction as a function of stimulus contrast for the same 2 neurons ($f_c = 5$ Hz). **B** and **F**: average spike train distances for the same stimuli as in **A** and **E**, respectively. **D** and **H**: average spike train distances for the same stimuli as in **C** and **G**, respectively. Model parameters were set as follows. **A–D**: $G_a = 17$ spikes/s, $G_c = 7$ spikes/s, $\tau_a = 6$ ms, $f_{\text{EOD}} = 375$ Hz, $r_{\text{base}} = 5$ spike/s, $n = 3$, $V_{\text{th}} = 80$ mV. **E–H**: $G_a = 165$ Hz, $G_c = 34$ Hz, $\tau_a = 2$ ms, $f_{\text{EOD}} = 575$ Hz, $r_{\text{base}} = 65$ spikes/s, $n = 3$, $V_{\text{th}} = 130$ mV.

period driven by the stimulus did not reproduce the spike train variability of P-receptor afferents. A comparison of variance versus mean spike count with theoretical results (Vannucci and Teich 1981) suggests that the regularizing effect of the refractory period is not sufficient to account entirely for the low variability observed in our data. In addition to the refractory period, the generation of spikes in P-receptor afferents appears to be governed by biophysical mechanisms that exhibit intermediate levels of variability lying between those of Poisson and perfect integrate-and-fire models and corresponding to the factors $n = 3$ –10 of our gamma models.

Because of their mathematical definition and properties, the distances $D_n(q)$ and the average timing jitter \bar{t}_{jitter} are well suited to characterize the reproducibility of spike occurrence times from one trial to the next. These measures are equally effective with deterministic or random stimuli and are applicable in cases, such as here, where simpler measures like the timing precision or reliability cannot be used (see Fig. 4) (Bair and Koch 1996; Berry et al. 1997). By definition, the average jitter \bar{t}_{jitter} is a measure that automatically incorporates possible differences in spike number between two spike trains. For example, since on average 23% of the spikes had to be added or deleted to transform one spike train to a second one in our data set (see RESULTS, *Quantification of response variability*, last paragraph), the average time interval by which the remaining spikes were moved was actually smaller by 15% than that reported in Fig. 8. This may be seen from Eqs. 3 and 4: if n_α and/or n_β are different from zero, the parenthesis on the right hand side of Eq. 4 will be smaller than one (0.85 in the present case), implying that $\bar{t}_{\text{jitter}} = 1/\bar{q}_{1/2}$ is larger than the average time interval given by the left hand side of Eq. 4. The additional 15% increase in \bar{t}_{jitter} converts the added or deleted spikes into an effective time jitter equivalent.

Our use of spike train distances is different from the one originally introduced by Victor and Purpura (1996, 1997). These authors employed spike train distances to assess the information conveyed by stimulus-dependent clustering of spike trains from neurons of the monkey visual cortex. In the present study, spike distances were used only to assess the variability across identical trials; the performance at conveying stimulus-dependent information was monitored with a second, independent measure, the coding fraction.

Variability under various stimulus conditions

The results illustrated in Figs. 9–12 show that the timing precision of P-receptor afferent spikes increases with the cutoff frequency of the stimulus and, to a lesser extent, with the contrast of the RAMs. These results are consistent with observations made in other preparations reporting that fast transients are likely to increase the precision of spike occurrence times (Berry et al. 1997; Mechler et al. 1998; Warzecha et al. 1998). Similarly, our findings that spike trains can be more reproducible at low than at high firing rates (see Fig. 4) is consistent with earlier observations (Berry et al. 1997; de Ruyter van Steveninck et al. 1997; Warzecha and Egelhaaf 1999). In contrast, no significant differences in reliability were observed for RAM or SAM stimuli. Under the assumption that the RAMs employed here are closer to natural stimuli than SAMs (de Ruyter van

Steveninck et al. 1997), our results do not support the idea that spike timing is more reliable under natural stimulation (Warzecha and Egelhaaf 1999). Behavioral experiments show that *Eigenmannia* is able to perform remarkably precise jamming avoidance behaviors under artificial stimulation (for a review, see Kawasaki 1997). Accordingly, the reliability of spike timing recorded in the time-coding pathway is very precise under such conditions. In contrast to the amplitude-coding pathway, high reliability in the time-coding pathway is necessary for the jamming avoidance response.

Variability and robustness of encoding

Our results show that the average jitter in the timing of P-receptor afferent spikes \bar{t}_{jitter} is in most cases below 4 ms. On the other hand, the robustness of encoding to spike time jitter yields values of $\sigma_{\text{jitter}}^{50}$ well above 4 ms for most of the behaviorally relevant range of stimulus cutoff frequencies (see Table 1). Even at high stimulus cutoff frequencies (e.g., $f_c = 60$ Hz), a jitter of 4 ms leads to a relative decrease in coding fraction of at most 18% (see Table 1; $\sigma_{\text{jitter}}^{50} = 11$ ms implies that $\gamma_n(4 \text{ ms}) = 0.82$). A similar observation is valid for spike additions and deletions. Therefore the jitter observed in P-receptor afferents is in a temporal range that does not significantly affect the information transmitted by single spike trains for most units and stimulus conditions. On the other hand, a small amount of spike time jitter is beneficial to improve the stimulus estimate obtained from several independent spike trains by averaging. We verified this by computing estimates of the stimulus from $n = 2$ –10 spike trains (recorded successively from one neuron) simultaneously (Kreiman et al. 1998). The coding fraction increased when additional spike trains were included and started to saturate for $n = 6$ –7 spike trains. Thus our results suggest that the spike timing jitter of P-receptor afferents lies in a range for which the information transmitted by single units (when assessed by linear estimation) is not degraded (for the range of behaviorally relevant stimulus cutoff frequencies considered here) but which still allows for improvement by averaging over a small number of afferents. Additional experiments recording simultaneously from several P-receptor afferents under repeated presentations of the same RAMs are needed to confirm this result.

Variability and the processing of AM in the electrosensory lateral line lobe (ELL)

At the next stage of the amplitude coding pathway, the information carried by P-receptor afferent spike trains is processed by pyramidal cells of the ELL. These neurons represent the output elements of the amplitude pathway and project to various higher order brain structures specialized in the processing of electrosensory information. There are two types of pyramidal cells, E- and I-type, which receive direct excitatory input and indirect input via inhibitory interneurons, respectively. At least two transformations have been identified in the representation of AMs between the afferent input and the pyramidal cell output to the ELL: 1) the detection threshold of pyramidal cells for AMs appears considerably lower than the one of P-receptor afferents (Bastian 1981) and 2) E- and I-type pyramidal cells appear less sensitive to the detailed time course

of AMs than P-receptor afferents and seem to extract the occurrence of upstrokes and downstrokes in AMs, respectively (Metzner et al. 1998). Both these transformations are likely to play a role in the generation of electrolocation and electrocommunication behaviors. In particular, understanding how the increased sensitivity of pyramidal cells arises might contribute to explain jamming avoidance responses to extremely weak AMs and the detection of small preys using the electric sense (Kawasaki 1997; Nelson and MacIver 1999).

Some sort of averaging operation across several afferent fibers converging onto a pyramidal cell is likely to contribute to this increased sensitivity (Bastian 1981), as discussed in the previous section. One biophysical mechanism specifically proposed to enhance the sensitivity of E-type pyramidal cells to upstrokes in the AM waveform is coincidence detection (Berman and Maler 1999): in slices of the ELL of *Apteronotus*, the stimulation of afferents in the deep fiber layer produces compound postsynaptic potentials consisting of an initial, fast-rising excitatory postsynaptic potential followed by an inhibitory postsynaptic potential that limits the time window of integration to <10 ms and could therefore act as a high-pass filter for coincident spikes occurring within 1–2 EOD cycles of each other (Berman and Maler 1998; see Softky 1995 for a similar theoretical result). Our experimental results show that under repeated RAM stimulation, more than 77% of P-receptor afferent spikes will on average occur within 1–2 EOD cycles of each other in response to the same AM (Fig. 8B). Thus within the range of stimulus parameters investigated in this study, spike trains of P-receptor afferents appear indeed able to provide the information necessary for such coincidence detection operations.

The authors thank Dr. M. Stopfer for carefully reading the manuscript and suggesting many improvements. Experiments were carried out by R. Krahe and W. Metzner. Data analysis was carried out by G. Kreiman and F. Gabbiani. F. Gabbiani and G. Kreiman co-wrote the paper. The original experiments were designed by F. Gabbiani, C. Koch, and W. Metzner.

This work was supported by a National Science Foundation grant to C. Koch and W. Metzner, by a National Institute of Mental Health grant to C. Koch, and by the Sloan Center for Theoretical Neuroscience.

REFERENCES

- BAIR W AND KOCH C. Temporal precision of spike trains in extrastriate cortex of the behaving macaque monkey. *Neural Comp* 8: 1185–1202, 1996.
- BARBERINI CL, HORWITZ GD, AND NEWSOME WT. A comparison of spiking statistics in motion sensing neurons of flies and monkeys. In: *Computational, Neural and Ecological Constraints of Visual Motion Processing*, edited by Zeil J and Zanker JM. Springer Verlag, In press.
- BASTIAN J. Electrolocation. II. The effects of moving objects and other electrical stimuli on the activities of two categories of posterior lateral line lobe cells in *Apteronotus albifrons*. *J Comp Physiol* 144: 481–494, 1981.
- BAYLOR DA, LAMB TD, AND YAU K-W. Responses of retinal rods to single photons. *J Physiol (Lond)* 288: 613–634, 1979.
- BERMAN NJ AND MALER L. Inhibition evoked from primary afferents in the electrosensory lateral line lobe of weakly electric fish (*Apteronotus leptorhynchus*). *J Neurophysiol* 80: 3173–3213, 1998.
- BERMAN NJ AND MALER L. Neural architecture of the electrosensory lateral line lobe: adaptations for coincidence detection, a sensory searchlight and frequency-dependent adaptive filtering. *J Exp Biol* 202: 1243–1253, 1999.
- BERRY MJ AND MEISTER M. Refractoriness and neural precision. *J Neurosci* 18: 2200–2211, 1998.
- BERRY MJ, WARLAND DK, AND MEISTER M. The structure and precision of retinal spike trains. *Proc Natl Acad Sci USA* 94: 5411–5416, 1997.
- BIALEK W, DE RUYTER VAN STEVENINCK R, AND WARLAND D. Reading a neural code. *Science* 252: 1854–1857, 1991.
- CARR C, HEILIGENBERG W, AND ROSE G. A time comparison circuit in the electric fish midbrain. I. Behavior and physiology. *J Neurosci* 6: 107–110, 1986.
- DE RUYTER VAN STEVENINCK R, LEWEN GD, STRONG SP, KOBERLE R, AND BIALEK W. Reproducibility and variability in neural spike trains. *Science* 275: 1805–1808, 1997.
- FUKUNAGA K. *Introduction to Statistical Pattern Recognition* (2nd ed.). San Diego, CA: Academic, 1990.
- GABBIANI F AND KOCH C. Coding of time-varying signals in spike trains of integrate-and-fire neurons with random threshold. *Neural Comput* 8: 44–66, 1996.
- GABBIANI F AND KOCH C. Principles of spike train analysis. In: *Methods in Neuronal Modeling* (2nd ed.), edited by Segev I and Koch C. Cambridge, MA: MIT Press, 1998, p. 313–360.
- GABBIANI F AND METZNER W. Encoding and processing of sensory information in neuronal spike trains. *J Exp Biol* 202: 1267–1279, 1999.
- HECHT S, SHLAER S, AND PIRENNE MH. Energy, quanta, and vision. *J Gen Physiol* 25: 819–840, 1942.
- HEILIGENBERG W. *Neural Nets in Electric Fish*. Cambridge, MA: MIT Press, 1991.
- JOHNSON DH. Point process models of single-neuron discharges. *J Comput Neurosci* 3: 275–299, 1996.
- KASHIMORI Y, GOTO M, AND KAMBARA T. Model of P- and T-electroreceptors of weakly electric fish. *Biophys J* 70: 2513–2526, 1996.
- KAWASAKI M. Sensory hyperacuity in the jamming avoidance response of weakly electric fish. *Curr Opin Neurobiol* 7: 473–479, 1997.
- KREIMAN G, GABBIANI F, METZNER W, AND KOCH C. Robustness of amplitude modulation encoding by P-receptor afferent spike trains of weakly electric fish. *Soc Neurosci Abstr* 24: 186, 1998.
- LI W-H AND GRAUR D. *Fundamentals of Molecular Evolution*. Sunderland, MA: Sinauer Associates, 1991.
- MAINEN ZF AND SEJNOWSKI TJ. Reliability of spike timing in neocortical neurons. *Science* 268: 1503–1506, 1995.
- MECHLER F, VICTOR JD, PURPURA KP, AND SHAPLEY R. Robust temporal coding of contrast by V1 neurons for transient but not for steady-state stimuli. *J Neurosci* 18: 6583–6598, 1998.
- METZNER W, KOCH C, WESSEL R, AND GABBIANI F. Feature extraction by burst-like spike patterns in multiple sensory maps. *J Neurosci* 18: 2283–2300, 1998.
- NELSON ME AND MACIVER MA. Prey capture in the weakly electric fish *Apteronotus albifrons*. *J Exp Biol* 202: 1205–1215, 1999.
- NELSON ME, XU Z, AND PAYNE JR. Characterization and modeling of P-type electrosensory afferent responses to amplitude modulations in a wave-type electric fish. *J Comp Physiol* 181: 532–544, 1997.
- PARKER AJ AND NEWSOME WT. Sense and the single neuron: probing the physiology of perception. *Annu Rev Neurosci* 21: 227–277, 1998.
- POOR HV. *An Introduction to Signal Detection and Estimation* (2nd ed.). New York: Springer, 1994.
- PRESS WH, TEUKOLSKY SA, VETTERLING WT, AND FLANNERY BP. *Numerical Recipes in C, The Art of Scientific Computing* (2nd ed.). Cambridge, UK: Cambridge Univ. Press, 1992.
- REICH DS, VICTOR JD, KNIGHT BW, OZAKI T, AND KAPLAN E. Response variability and timing precision of neuronal spike trains in vivo. *J Neurophysiol* 77: 2836–2841, 1997.
- ROSE G AND HEILIGENBERG W. Temporal hyperacuity in the electric sense of fish. *Nature* 318: 178–180, 1985.
- SCHEICH H, BULLOCK TH, AND HAMSTRA RH. Coding properties of two classes of afferent nerve fibers: high-frequency electroreceptors in the electric fish *Eigenmannia*. *J Neurophysiol* 36: 39–60, 1973.
- SELLERS PH. On the theory and computation of evolutionary distances. *SIAM J Appl Math* 26: 787–793, 1974.
- SHADLEN MN, BRITTEN KH, NEWSOME WT, AND MOVSHON JA. A computational analysis of the relationship between neuronal and behavioral responses to visual motion. *J Neurosci* 16: 1486–1510, 1996.
- SOFTKY WR. Simple codes versus efficient codes. *Curr Biol* 5: 239–247, 1995.
- SOFTKY WR AND KOCH C. The highly irregular firing of cortical cells is inconsistent with temporal integration of EPSPs. *J Neurosci* 13: 334–350, 1993.
- STEVENS CF AND ZADOR AM. Input synchrony and the irregular firing of cortical neurons. *Nature Neurosci* 1: 210–217, 1998.
- TEICH MC, TURCOTT RG, AND SIEGEL RM. Temporal correlation in cat striate-cortex neural spike trains. *IEEE Eng Med Biol Sept/Oct*: 79–87, 1996.
- VANNUCCI G AND TEICH MC. Dead-time-modified photocount mean and variance for chaotic radiation. *J Opt Soc Am* 71: 164–170, 1981.

- VICTOR JD AND PURPURA KP. Nature and precision of temporal coding in visual cortex: a metric-space analysis. *J Neurophysiol* 76: 1310–1326, 1996.
- VICTOR JD AND PURPURA KP. Metric-space analysis of spike trains, algorithms and application. *Network: Comput Neural Systems* 8: 127–164, 1997.
- WARZECHA AK AND EGELHAAF M. Variability in spike trains during constant and dynamic stimulation. *Science* 283: 1927–1930, 1999.
- WARZECHA AK, KRETZBERG J, AND EGELHAAF M. Temporal precision of the encoding of motion information by visual interneurons. *Curr Opin Neurobiol* 8: 359–368, 1998.
- WESSEL R, KOCH C, AND GABBIANI F. Coding of time-varying electric field amplitude modulations in a wave-type electric fish. *J Neurophysiol* 75: 2280–2293, 1996.